Noise-Induced Front Motion: Signature of a Global Bifurcation

J. Hizanidis,[1] A. Balanov,[1,2] A. Amann,[1,3] and E. Schöll[1]

[1]*Institut für Theoretische Physik, Technische Universität Berlin, Hardenbergstraße 36, 10623 Berlin, Germany*
[2]*School of Physics and Astronomy, University of Nottingham, Nottingham NG7 2RD, United Kingdom*
[3]*Tyndall National Institute, Lee Maltings, Cork, Ireland*

(Received 17 November 2005; published 23 June 2006)

We show that front motion can be induced by noise in a spatially extended excitable system with a global constraint. Our model system is a semiconductor superlattice exhibiting complex dynamics of electron accumulation and depletion fronts. The presence of noise induces a global change in the dynamics of the system forcing stationary fronts to move through the entire device. We demonstrate the effect of coherence resonance in our model; i.e., there is an optimal level of noise at which the regularity of front motion is enhanced. Physical insight is provided by relating the space-time dynamics of the fronts with a phase-space analysis.

DOI: 10.1103/PhysRevLett.96.244104 PACS numbers: 05.45.−a, 05.40.−a, 73.21.Cd

Theoretical and experimental research has recently shown that noise can have surprisingly constructive effects in many physical systems. In particular, an optimal noise level may give rise to ordered behavior and even produce new dynamical states [1]. In spite of considerable progress on a fundamental level, useful applications of noise-induced phenomena in technologically relevant devices are still scarce.

Here we study the influence of noise on the electron dynamics of a semiconductor superlattice. We choose this particular system for the following reasons: (i) It models a concrete and well studied [2–4] physical system with a rich dynamical behavior; experimental verification as well as technological exploitation of noise-induced phenomena are therefore in principle possible. Semiconductor nanostructure devices are practically relevant nonlinear model systems [5] and the superlattice, in particular, can serve in applications as an ultrahigh frequency electronic oscillator [6,7]. (ii) The noise arises naturally, due to the probabilistic nature of the tunneling current, thermal fluctuations, etc. (iii) The superlattice system may serve as an exemplary model system for the concept of noise-induced front motion under a global constraint. In fact, the deterministic bifurcation scenario shows signs of universality [8,9], and similar deterministic front dynamics occurs in many physical, chemical, and biological systems [10–12].

We develop a stochastic model for a superlattice which consists of epitaxial layers of two semiconductor materials with different band gaps, thus forming a periodic sequence of potential wells and barriers. Our model is based on sequential tunneling of electrons [3]. The resulting tunneling current density $J_{m\to m+1}(F_m, n_m, n_{m+1})$ from well m to well $m+1$ depends only on the electric field F_m between both wells and the electron densities n_m and n_{m+1} in the respective wells (in units of cm^{-2}), as given by Eqs. (83) and (86) in Ref. [3]. In order to take into account various sources of noise, we approximate the random fluctuations of the current densities by additive Gaussian white noise $\xi_m(t)$ with $\langle \xi_m(t)\rangle = 0$ and $\langle \xi_m(t)\xi_{m'}(t')\rangle = \delta(t-t')\delta_{mm'}$, which yields the following Langevin equations:

$$e\frac{dn_m}{dt} = J_{m-1\to m} + D\xi_m(t) - J_{m\to m+1} - D\xi_{m+1}(t), \quad (1)$$

where D is the noise intensity. Since the interwell coupling in our superlattice model is very weak and the tunneling times are much smaller than the characteristic time scale of the global current $J = \frac{1}{N+1}\sum_{m=0}^{N} J_{m\to m+1}$, these noise sources can be treated as uncorrelated both in time and space. Charge conservation is automatically guaranteed by adding a noise term ξ_m to each current density $J_{m-1\to m}$. The physical origin of the noise may be, e.g., thermal noise, $1/f$ noise, or shot noise due to the randomly fluctuating tunneling times of discrete charges across the barriers. The latter is Poissonian and can be approximated by $D = (eJ_{m-1\to m}/A)^{1/2}$ [4,13], which increases with decreasing current cross section A; thus this type of noise dominates for small devices, while thermal noise dominates for higher temperature. In the following we summarize the global effect of noise by a constant D.

The electron densities and the electric fields are coupled by the discrete Poisson equation:

$$\epsilon_r\epsilon_0(F_m - F_{m-1}) = e(n_m - N_D) \quad \text{for} \quad m = 1, \ldots, N, \quad (2)$$

where ϵ_r and ϵ_0 are the relative and absolute permittivities, $e < 0$ is the electron charge, N_D is the doping density, and F_0 and F_N are the fields at the emitter and collector barrier, respectively. In the deterministic case, i.e., at $D = 0$, the various dynamical scenarios include formation of charge accumulation and depletion fronts associated with stationary, periodic, or even chaotic current oscillations [8,9,14]. The two control parameters which are crucial for the patterns to be observed are the applied voltage U between emitter and collector, which gives rise to a global constraint,

$$U = -\sum_{m=0}^{N} F_m d, \tag{3}$$

where d is the superlattice period, and the contact conductivity σ. We use Ohmic boundary conditions, $J_{0\to1} = \sigma F_0$ and $J_{N\to N+1} = \sigma F_N \frac{n_N}{N_D}$.

In the following we choose the control parameters U and σ such that the deterministic system exhibits no oscillations. The system is prepared at a stable fixed point which corresponds to a stationary accumulation front [Fig. 1(a)]. As the noise intensity is increased, the behavior of the system changes dramatically [Figs. 1(b) and 1(c)]: the accumulation front remains stationary only for a while, until a pair of a depletion and another accumulation front (i.e., a charge dipole with a high-field domain in between) is generated at the emitter. As is known from the deterministic system, this dipole injection depends critically upon the emitter current [9]. Here it is triggered by noise at the emitter [15]. Because of the global voltage constraint (3) the growing dipole field domain between the injected depletion and accumulation fronts requires the high-field domain between the stationary accumulation front and the collector to shrink, and hence that accumulation front starts moving towards the collector. For a short time there are two accumulation fronts and one depletion front in the sample, thereby forming a tripole [16], until the first accumulation front reaches the collector and disappears. When the depletion front reaches the collector, the remaining accumulation front must stop moving because of the global constraint (3), and this happens at the position where the first accumulation front was initially localized. After some time, noise generates another dipole at the emitter and the same scenario is repeated.

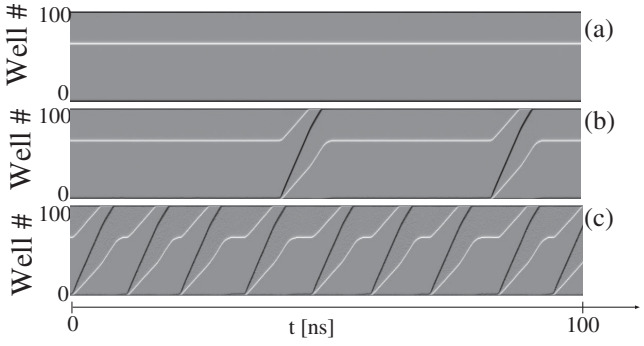

FIG. 1. Noise-induced front motion: Space-time plots of the electron density for (a) $D = 0$ (no noise), (b) $D = 0.5$ A s$^{1/2}$/m^2, and (c) $D = 2.0$ A s$^{1/2}$/m^2. Light and dark shading corresponds to electron accumulation and depletion fronts, respectively. The emitter is at the bottom. Parameters: $U = 2.99$ V, $\sigma = 2.082\,101\,248\,8\ \Omega^{-1}\,\mathrm{m}^{-1}$, $N_D = 10^{11}$ cm^{-2}, $T = 20$ K, $N = 100$ GaAs wells of width $w = 8$ nm, and $Al_{0.3}Ga_{0.7}As$ barriers of width $b = 5$ nm, energies $E^a = 41.5$ meV, $E^b = 160$ meV, scattering width $\Gamma = 8$ meV, transition matrix elements $H^{a,b}_{m,m+1} = -eF_m \times 0.0127$ m, $H^{a,a}_{m+1,m} = -0.688$ meV, $H^{b,b}_{m+1,m} = 1.263$ meV, as in Ref. [9].

There are two distinct time scales in the system. One is related to the time the depletion front takes to travel through the superlattice. The other time scale is associated with the time needed for a new depletion front to be generated at the emitter. These two time scales are also visible in the noise-induced current oscillations; see Fig. 2(a). The time series of the current density are in the form of a pulse train with two characteristic times: the activation time, which is the time needed to excite the system from this stable fixed point (time needed for a new depletion front to be generated at the emitter), and the excursion time, which is the time needed to return from the excited state to the fixed point (time the depletion front needs to travel through the device). Low noise is associated with large activation times and small, almost constant, excursion times, while as the noise level increases, activation times become smaller and at sufficiently large D vanish.

At low D the spike train looks irregular, and the interval between excitations (mean interspike interval $\langle T\rangle$) is relatively large and random in time. At moderate noise, the spiking is rather regular, therefore suggesting that the mean interspike interval does not vary substantially. Further increase of noise results in a highly irregular spike train with very frequent spikes. In Fig. 2(b) (top panel) the decrease of $\langle T\rangle$ as a function of D is shown thus demonstrating that the mean interspike interval is strongly controlled by the noise intensity. This is very important in terms of experiments, where noise can induce oscillations by forcing stationary fronts to move. The corresponding spectral peak frequency f shows a linear scaling for small D. As a measure for coherence we use the normalized fluctuations of pulse duration $R_T = (\langle T^2\rangle - \langle T\rangle^2)^{1/2}/\langle T\rangle$ [17]. This quantity, as seen in Fig. 2(b) (bottom panel), is a nonmonotonic function of D, exhibiting a minimum at mod-

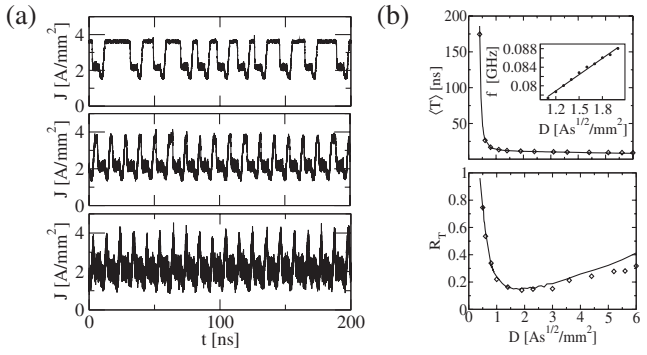

FIG. 2. (a) Three noise realizations of the current density $J(t)$. From top to bottom, $D = 0.8$, $D = 2.0$, and $D = 5.0$ A s$^{1/2}$/m^2. (b) Mean interspike interval (top panel) and its normalized fluctuations R_T (bottom panel) versus noise intensity. Lines, constant D; diamonds, $D \sim J^{1/2}_{m-1\to m}$ [18]. The inset shows the peak frequency versus D.

erate noise intensity [18]. This phenomenon is well known as *coherence resonance* [17,19,20], has been observed in various models, and is strongly connected to excitability. In order to find the origin of excitability in our system a stability analysis in a wide range of the control parameters has been done, setting $D = 0$.

Figure 3 shows a bifurcation diagram in the (σ, U) control parameter plane. The regime of oscillations is bounded below by a Hopf bifurcation (solid line), and above by a sawtoothlike boundary (cf. lower inset) where each tongue (dark gray or green) corresponds to a specific position of the stable accumulation front within the superlattice. With increasing U the position shifts towards the emitter, well by well, thus increasing the size of the high-field domain between the accumulation front and the collector. The parameters used in Figs. 1 and 2 correspond to the tongue labeled 64. Increasing U at fixed σ, the stable fixed point, which is associated with a stationary current density, collides with a saddle point and is replaced by a limit cycle of approximately constant amplitude and increasing frequency, corresponding to tripole oscillations in the space-time diagram. Plotting the frequency of these oscillations versus the bifurcation parameter U, we obtain the characteristic *square-root scaling law* that governs a saddle-node bifurcation on a limit cycle (upper inset of Fig. 3). At the critical point U_{crit} the frequency of the oscillations tends to zero. This corresponds to an infinite period oscillation, and therefore this bifurcation is also known as saddle-node infinite period bifurcation or SNIPER [21]. In semiconductors it has been previously found for Gunn domains in bulk material [22] as well as in superlattices with strong disorder [23]. Figure 4(a) shows a phase portrait in terms of electron densities in two neighboring wells, below the bifurcation. The electron density in well 65, n_{65}, is plotted versus n_{64}, in a projection of the 100-dimensional phase space. Arrows denote the direction that the trajectory follows, and the thick dot (VI) corresponds to the stable node (i.e., a stationary accumulation front) that all trajectories approach regardless of the initial condition. The cross denotes the saddle point which corresponds to a stationary spatial configuration which separates two regimes: Either *no* dipole is injected at the emitter (this is associated with the *short* piece of the unstable manifold connecting the saddle and the stable node), or a dipole is injected and traverses the system, and interacts with the stationary accumulation front, thus performing a full tripole oscillation. The latter corresponds to the trajectory shown (labeled I–V), which performs a large excursion in phase space before approaching the stable node (VI). It is close to the *long* piece of the unstable manifold connecting the saddle with the node via a big loop. In Figs. 4(b) and 4(c) the space-time plot of the electron densities and the time evolution of the electron density n_{65}, respectively, are plotted for the same trajectory. From Fig. 4(b) we see that initially an accumulation front is located near well 64 (I). After a depletion front is injected at the emitter, followed immediately by the injection of an accumulation front, both move through the system (II–IV) while the first accumulation front also starts moving towards the collector (II) (driven by the global constraint). Finally the accumulation front generated at the emitter approaches well 64 (V) and rests there (VI), while at the emitter a new depletion front starts to develop. In this context the previously discussed saddle point corresponds to the stationary but unstable situation, where the depletion front is not yet completely detached from the emitter.

The global bifurcation can be understood by noting the important role of the current at the emitter for the bifurca-

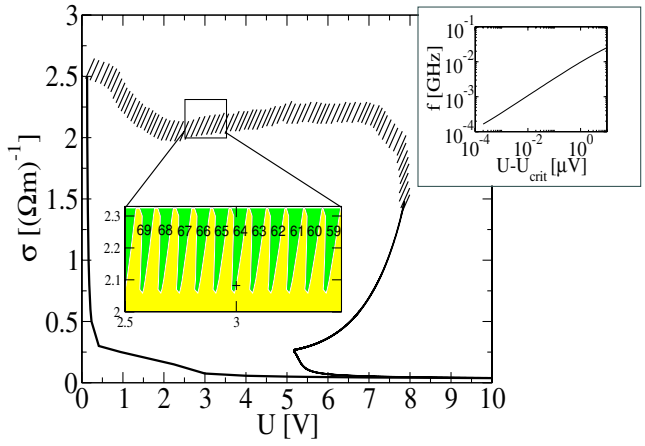

FIG. 3 (color online). Bifurcation diagram in the (σ, U) plane. Thick or hatched lines mark the transition from stationary to moving fronts via a Hopf or a saddle-node bifurcation on a limit cycle, respectively. The inset shows a blowup of a small part of the hatched line revealing its sawtoothlike structure. Dark (green) and light (yellow) regions correspond to stationary and moving fronts, respectively, where the numbers denote the positions of the stationary accumulation front in the superlattice. Upper inset shows the frequency f of the limit cycle which is born above the critical point (marked by a cross in the lower inset) as function of U.

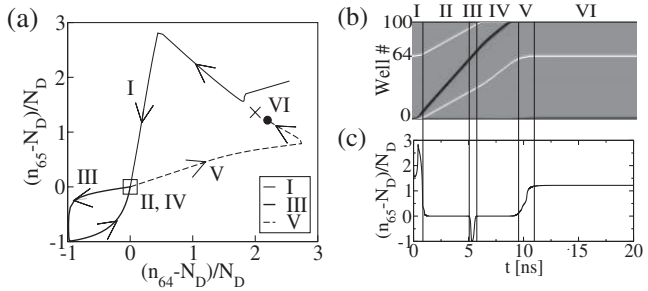

FIG. 4. (a) Phase portrait in terms of electron densities n_{65} and n_{64}, normalized to the donor density N_D, below the global bifurcation. (b) Space-time plot and (c) time series of n_{65} for the trajectory shown in (a). The different parts of the trajectory are labeled by roman numerals I–VI in (a), (b), and (c). Parameters as in Fig. 1, $D = 0$.

tion. For high σ only stationary accumulation fronts appear, and a typical sawtooth pattern in the current-voltage characteristic is obtained [23]. As we decrease σ, we lower the critical current J_c, above which depletion fronts are triggered at the emitter [9]. In the regime of σ, shown in the lower inset of Fig. 3, it depends upon the voltage whether a depletion front will develop fully at the emitter. In the dark (green) region the current of the stationary accumulation front is below J_c, and therefore no fronts are generated at the emitter. In the region of the light (yellow) tongues, however, the stationary accumulation front is not stable, since it corresponds to a current larger than J_c. Instead of a stationary current we therefore observe periodic current oscillations, where the current rises above J_c only during the dipole injection phases, and otherwise is less than J_c [9]. This is the physical interpretation of the SNIPER in the deterministic picture, which helps one to better understand the effect noise has when added to the system. In fact, sufficiently strong noise drives the system away from the stable node (VI) across the saddle, whence it returns to VI via a tripole oscillation as shown in Fig. 1.

In conclusion, we have shown that noise is able to induce quite regular charge front motion in a semiconductor superlattice. Noise triggers the injection of fronts into the system and thus determines the frequency of the resulting current oscillations, whereas the front propagation velocity is insensitive to the noise level. This opens promising applications of superlattices as fast noise sensors which convert the noise intensity into frequency. Such sensors could potentially be used for measuring temperature, pressure, electromagnetic bias, or other parameters which affect the level of noise in a superlattice. Of course, those parameters would also affect the deterministic state of the system. However, since the sensitivity of the mean interspike interval and thus of the mean frequency upon the noise intensity is particularly strong for small noise intensity near the coherence resonance [cf. Fig. 2(b), top panel], this effect can be expected to dominate as long as no other bifurcations are induced. Thus, further experimental study would be very interesting. The results are also important from the point of view of nonlinear dynamics, since they uncover a mechanism of excitability which can occur in an extended system under a global constraint. The noise-induced front motion reveals the signature of a global bifurcation, namely, a saddle-node bifurcation on a limit cycle present in the deterministic system, and shows coherence resonance.

This work was supported by DFG in the framework of Sfb 555. We thank N. Janson for stimulating discussions and help with the stability analysis.

[1] J. García-Ojalvo and J. M. Sancho, *Noise in Spatially Extended Systems* (Springer, New York, 1999).
[2] L. Esaki and L. L. Chang, Phys. Rev. Lett. **33**, 495 (1974).
[3] A. Wacker, Phys. Rep. **357**, 1 (2002).
[4] L. L. Bonilla and H. T. Grahn, Rep. Prog. Phys. **68**, 577 (2005).
[5] E. Schöll, *Nonlinear Spatio-Temporal Dynamics and Chaos in Semiconductors* (Cambridge University Press, Cambridge, England, 2001).
[6] J. Kastrup *et al.*, Phys. Rev. B **52**, 13 761 (1995).
[7] K. Hofbeck *et al.*, Phys. Lett. A **218**, 349 (1996).
[8] A. Amann, K. Peters, U. Parlitz, A. Wacker, and E. Schöll, Phys. Rev. Lett. **91**, 066601 (2003).
[9] A. Amann and E. Schöll, J. Stat. Phys. **119**, 1069 (2005).
[10] A. S. Mikhailov, *Foundations of Synergetics* (Springer, Berlin, 1994), 2nd ed., Vol. I.
[11] *Chemical Waves and Patterns*, edited by R. Kapral and K. Showalter (Kluwer, Dordrecht, 1995).
[12] J. Müller and W. van Saarloos, Phys. Rev. E **65**, 061111 (2002).
[13] Y. M. Blanter and M. Büttiker, Phys. Rep. **336**, 1 (2000).
[14] A. Amann, J. Schlesner, A. Wacker, and E. Schöll, Phys. Rev. B **65**, 193313 (2002).
[15] We have in fact verified that the same scenarios occur if noise is applied locally only to the wells near the emitter.
[16] A. Amann, A. Wacker, and E. Schöll, Physica (Amsterdam) **314B**, 404 (2002).
[17] A. Pikovsky and J. Kurths, Phys. Rev. Lett. **78**, 775 (1997).
[18] To check if our results are affected by using shot noise terms $D_m(t) \sim [J_{m-1\to m}(t)]^{1/2}$ instead of constant D, we have repeated all simulations such that the stationary value of $D_m(t)$ equals D. The results [diamonds in Fig. 2(b)] coincide very well with our simple noise model, since the noise-sensitive part of the time-dependent trajectory is close to the stationary state. Note that $D = 1\ \mathrm{A\,s^{1/2}/m^2}$ corresponds to shot noise with $A \approx 1\ \mu\mathrm{m}^2$.
[19] H. Gang, T. Ditzinger, C. Ning, and H. Haken, Phys. Rev. Lett. **71**, 807 (1993).
[20] A. Longtin, Phys. Rev. E **55**, 868 (1997).
[21] J. Guckenheimer and P. Holmes, *Nonlinear Oscillations, Dynamical Systems, and Bifurcations of Vector Fields* (Springer, Berlin, 1986).
[22] Y. H. Shiau and Y. C. Cheng, Solid State Commun. **99**, 305 (1996).
[23] M. Patra, G. Schwarz, and E. Schöll, Phys. Rev. B **57**, 1824 (1998).